IEEE Open Journal of
Power Electronics

Received 22 July 2020; accepted 10 August 2020. Date of publication 17 August 2020;
date of current version 5 October 2020. The review of this article was arranged by Associate Editor Lijun Hang.

Digital Object Identifier 10.1109/OJPEL.2020.3016942

An Ellipse-Optimized Composite Backstepping Control Strategy for a Point-of-Load Inverter Under Load Disturbance in the Shipboard Power System

JINSONG HE [1] (Student Member, IEEE), AND XIN ZHANG [2] (Senior Member, IEEE)

[1] School of Electrical and Electronic Engineering, Nanyang Technological University, Singapore 639798, Singapore
[2] College of Electrical Engineering, Zhejiang University, Hangzhou 310027, China

CORRESPONDING AUTHOR: XIN ZHANG (e-mail: jackzhang@ntu.edu.sg)

This work is supported by the Start-up grant of Professor Zhang Xin at Zhejiang University.

ABSTRACT The shipboard power system (SPS) is expected to be configured as a hybrid microgrid (MG) to realize redundant bus design and high penetration of renewables (REs). Point-of-load (POL) inverters in SPSs play a critical role to feed for sensitive ac load. To realize voltage-oriented control objective under load disturbance due to load uncertainty or nonlinearity, this paper proposes an ellipse-optimized composite back-stepping control strategy for a POL inverter. Firstly, the backstepping algorithm is harnessed to derive the pseudo-inductor-current-loop reference and decoupled switching functions in *d*-*q* frame, which can rigorously guarantee the global large-signal stability of the system. A Kalman filter is designed to estimate the load current and feedforward it to the backstepping controller for load disturbance rejection, saving three current sensors. The controller gains are quantitatively selected to achieve the optimal system damping and maximized dynamic response, which can be intuitively interpreted via an ellipse-based strategy from a geometrical point of view. Rigorous stability proof and robustness analysis of the system is also provided. Finally, simulation and experimental results verify the effectiveness of the proposed control scheme.

INDEX TERMS Microgrid, large-signal stability, backstepping, Lyapunov, Kalman filter, feedforward, optimal control.

NOMENCLATURE

E	dc-link voltage
$\omega = 2\pi f$	Fundamental angular frequency ($100\,\pi$)
L, C	Nominal filter inductance, capacitance
v_{od}, $v_{oq}(x_1, x_3)$	Load voltages in d, q frames
i_{Ld}, $i_{Lq}(x_2, x_4)$	Inductor currents in d, q frames
i_{od}, i_{oq}	Load currents in d, q frames
x_1^*, x_3^*	Load-voltage references in d, q frames
v_m	Desired load-voltage amplitude
$x_2{}^*$, $x_4{}^*$	Inductor-current references in d, q frames
z_1, z_3	Load voltage tracking errors in d, q frames
z_2, z_4	Current tracking errors in d, q frames
V_1, V_2	Defined Lyapunov functions in d frame
V_3, V_4	Defined Lyapunov functions in q frame
$\dot{V}(\mathrm{d}V/\mathrm{d}t)$	First-order time derivative of V
μ_d, μ_q	Switching functions in d, q frames
k_1, k_2, k_3, k_4	Controller gains (>0)
k_1^*, k_2^*	Optimized controller gains
λ_1, λ_2	Solutions of the characteristic equation
ω_n	The equivalent natural resonance frequency
ξ	Equivalent damping ratio
S_{MNOP}	The area of the rectangle $\square_{MNOP}$.
A, B, C	System matrixes of the state-space model
G	Feedback gain matrix of the Kalman filter
V_o, V_c	Lyapunov functions for robustness analysis

I. INTRODUCTION

Electrification of the shipboard power system (SPS) has started ever-faster change both for surface and submarine applications with different uses and tonnages recently [1].

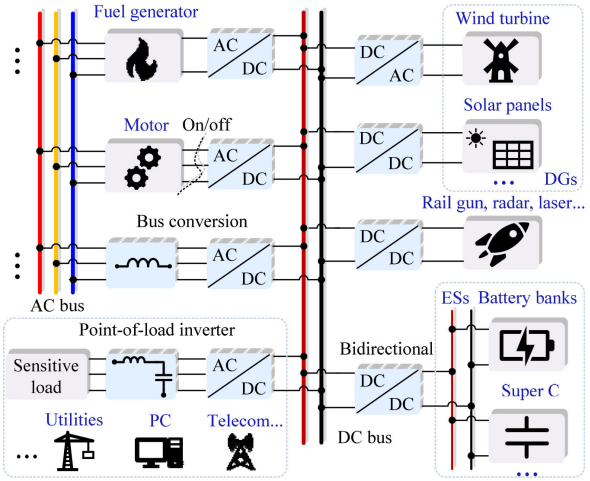

FIGURE 1. Investigated hybrid MG in the shipboard power systems (SPS).

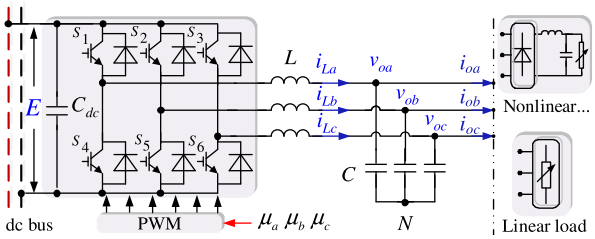

FIGURE 2. Investigated POL inverter system in the hybrid MG of the SPS.

The hybrid microgrid (MG) technology serves as the most promising technique to realize such up-gradation with improved system efficiency, reliability, and resilience [2]. As shown in Fig. 1, the hybrid MG in the SPS is an islanded mobile entity that integrates distributed generations (DGs), energy storage systems (ESs) and dc & ac consumptive ends together. In the hybrid MG, the bus conversion stage interlinks the ac MG subsystem and the dc MG subsystem together [3]. Such a dual-bus comprehensive system achieves redundancy design and combines the strength of ac MG and dc MG as well.

In the hybrid MG of the SPS, sensitive ac loads exist, such as the telecommunication facilities, computers, which cannot operate normally unless load voltage with high power quality is supplied. For this reason, they can hardly be driven by the ac bus directly due to the voltage sag/unbalance, harmonics, and electromagnetic interference (EMI), that promote the birth of the point-of-load inverter (POL) system [4].

As depicted in Fig. 2, the POL inverter is susceptible to load disturbance due to load uncertainty/nonlinearity. Meanwhile, it operates in complex and harsh environmental conditions. The varying temperatures, moistures, and air salinity inevitably cause plant parametric variations. To realize load voltage-oriented control objective under load disturbance and plant parametric uncertainty, advanced control schemes should be devised with full consideration of system stability, reliability, power density, and the implementation cost.

Conventional linear control methods, including proportional integral derivative (PID) control and proportional resonant (PR) control, have been widely used both in academia and industry in the past decades [5]. They have valid mature tools for controller gains selection, including but not limited to the Nyquist criterion, gain margin, and phase margin based on bode plot [6]. However, linear approaches are based on the small-signal model of the system in the vicinity of specific operation points [7]. Thus, only the local stability of the closed-loop system can be guaranteed around the operation point [8]. Once the POL inverter system is exposed to large perturbations away from the operation point, system stability may be deteriorated. Furthermore, linear approaches merely expect linear behavior of the closed-loop system that does not thoroughly leverage the system's full potential, leading to limited dynamic response.

To achieve a better dynamic response, nonlinear control methods emerge. In [9], conventional integer PID control is elevated to fractional-order PID control with greatly enhanced tracking accuracy and dynamic response. However, tuning of the controller gains is the current obstacle due to the mutual coupling effect. Model predictive control (MPC) is known for its great dynamic performance at the cost of comparatively high computation burden [10]. Apart from this, MPC lacks a commonly acknowledged effective method to tune the weighting factor so far. Dead-beat control is devised in a discrete-time domain, which could theoretically ensure zero steady-state error regulation with minimum rise time by assigning its poles at the origin of the z plane. However, it is comparatively sensitive to plant parameter uncertainty with an inherent two-step digital delay [11]. Sliding-mode control is robust against plant parametric variations but suffers from the chattering phenomenon [12]. Repetitive control is an expert at tracking/rejecting periodic reference/disturbance, but it is accompanied by relatively long internal time delay [13].

The above nonlinear approaches are devised from different perspectives with case-by-case advantages and defects. While they have two limitations in common. For one thing, they fail to rigorously guarantee the large-signal stability of the system. For another, it lacks effective valid guidelines for controller parameter selection, not to mention their optimization.

To ensure the large-signal stability of the system, Lyapunov-based control emerges, which is designed based on an all-in-one Lyapunov function (V) according to the direct method of Lyapunov's theory. In conventional Lyapunov-based control, the pseudo control variables' reference and switching function are selected to ensure $\mathrm{d}V/\mathrm{d}t < 0$ [14]. However, the derived final control law merely has a single current control loop [15], [16]. When extended for the POL inverter regulation, the load voltage is accompanied by steady-state error and sluggish dynamic response. To address this problem, [17] artificially imports the filter capacitor voltage feedback so that a dual-loop control scheme can be realized. However, this action fails to rigorously guarantee the negative definiteness of $\mathrm{d}V/\mathrm{d}t$, which means the large-signal stability cannot be always ensured. It also requires load-current sensors for practical

implementation. Recently, adaptive control is reported in [18]. It inherently has dual control loops to achieve better steady-state and transient performance, which could also rigorously guarantee the large-signal stability unconditionally. Meanwhile, it obviates the requirement of load-current sensors.

However, the design of V in the above Lyapunov-based control has no explicit rules. Comparatively, backstepping control provides a systematic way to construct the Lyapunov function, which contributes to derive the pseudo control variables' reference and final control law within finite recursive steps [19].

Besides, the controller gains selection guideline in [16]–[18] are just qualitatively illustrated without quantitative formulas. Currently, methods to optimize the controller gains in nonlinear control are still on the way. The trial-and-error method is straightforward but onerous and time-consuming [20]. After linearization around the equilibrium point, conventional linear tools can be implemented, such as eigenvalue analysis, root-locus technique, and bode plot [21]. Artificial intelligence (AI) aide method is a promising technique, involved with advanced algorithms and complicated on-line or off-line training process, such as particle swarm optimization (PSO) algorithm, multivariable multi-objective genetic algorithm (MMGA) [9], artificial neural network (ANN) [22], etc. However, the above approaches do not provide explicit formulas to select the controller gains. When extended for systems with different parameters, the whole tuning process requires to be repeated.

Motivated by the limitations of the above methods, this paper proposes an ellipse-optimized composite backstepping control scheme to regulate the POL inverter in the SPS, whose main contributions can be summarized as three points:

1) The composite backstepping controller inherently has decoupled dual control loops, that could rigorously guarantee the large-signal stability of the system.
2) To compensate for the load disturbance, a Kalman filter is designed to estimate and feedforward the load currents to the backstepping controller in the replacement of three current sensors, resulting in minimized implementation cost and enhanced system reliability.
3) An intuitive ellipse-based strategy with explicit formulas is proposed to optimize the controller gains, which not only theoretically achieves the optimal system damping and maximized dynamic response, but also helps select the feedback gain matrix of the Kalman filter quantitatively. Robustness analysis of the proposed control scheme has been incorporated both theoretically and experimentally.

II. PRELIMINARY OF THE ELLIPSE-OPTIMIZED COMPOSITE BACKSTEPPING CONTROLLER: MATHEMATICAL MODELLING

A. DYNAMIC EQUATIONS OF THE INVESTIGATED POL INVERTER

As shown in Fig. 2, according to Kirchhoff's circuit law and Kirchhoff's voltage law, the dynamic equation of the three-phase balanced system in vector-based form can be expressed as

$$L\frac{d\mathbf{i}_{Labc}}{dt} = \frac{1}{2}\mu_{abc}E - \mathbf{v}_{oabc} \quad C\frac{d\mathbf{v}_{oabc}}{dt} = \mathbf{i}_{Labc} - \mathbf{i}_{oabc} \tag{1}$$

where $\mathbf{i}_{Labc}$, $\mathbf{v}_{oabc}$, $\mathbf{i}_{oabc}$, $\boldsymbol{\mu}_{abc}$ denote the vectors of the filter inductor currents $[i_{La}\ i_{Lb}\ i_{Lc}]^T$, filter capacitor voltages $[v_{oa}\ v_{ob}\ v_{oc}]^T$, load currents $[i_{oa}\ i_{ob}\ i_{oc}]^T$ and switching functions $[\mu_a\ \mu_b\ \mu_c]^T$, composed of balanced three-phase individual quantities.

In comparison with the three-phase ac quantifies in *abc* frame, compatible state variables in the synchronous rotating reference frame (*d-q* frame) are dc quantities, which is much easier to be regulated. With the help of *abc-dq* coordinate transformation, (1) is transformed to *d-q*-frame counterpart, expressed as

$$\begin{cases} L\frac{di_{Ld}}{dt} = \frac{1}{2}\mu_d E - v_{od} + \omega L i_{Lq} \\ L\frac{di_{Lq}}{dt} = \frac{1}{2}\mu_q E - v_{oq} - \omega L i_{Ld} \end{cases}$$
$$\begin{cases} C\frac{dv_{od}}{dt} = i_{Ld} - i_{od} + \omega C v_{oq} \\ C\frac{dv_{oq}}{dt} = i_{Lq} - i_{oq} - \omega C v_{od} \end{cases} \tag{2}$$

where $\omega = 2\pi f = 100\ \pi$ denotes the fundamental angular frequency.

For the convenience of representation and derivation, the following equivalent substitution is performed, given by

$$x_1 = v_{od} \quad x_2 = i_{Ld}$$
$$x_3 = v_{oq} \quad x_4 = i_{Lq} \tag{3}$$

which transforms (2) into

$$C\dot{x}_1 = x_2 - i_{od} + \omega C x_3 \tag{4}$$
$$L\dot{x}_2 = 0.5\mu_d E - x_1 + \omega L x_4 \tag{5}$$
$$C\dot{x}_3 = x_4 - i_{oq} - \omega C x_1 \tag{6}$$
$$L\dot{x}_4 = 0.5\mu_q E - x_3 - \omega L x_2 \tag{7}$$

B. CONTROL OBJECTIVES: LOAD VOLTAGE REFERENCES x_1^*, x_3^*

The control objective is to regulate the three-phase load voltage to be purely sinusoidal. To fulfill this objective, x_1, x_3 are forced to track their dc references (x_1^*, x_3^*) respectively,

$$\begin{cases} x_1 \to x_1^* = v_m \\ x_3 \to x_3^* = 0 \end{cases} \tag{8}$$

III. RECURSIVE DERIVATION AND IMPLEMENTATION OF THE PROPOSED COMPOSITE BACKSTEPPING CONTROLLER

A. TWO-STEP BACKSTEPPING DERIVATION IN d FRAME

1) STEP ONE: DERIVATION OF INDUCTOR CURRENT REFERENCE x_2^*

Initially, load voltage tracking error in d frame is defined as

$$z_1 = x_1^* - x_1 \tag{9}$$

The first Lyapunov function associated with the defined load voltage tracking error in d frame is defined as

$$V_1 = \frac{1}{2}{z_1}^2 \tag{10}$$

Differentiating (10), it yields out that

$$\dot{V}_1 = z_1 \dot{z}_1 \tag{11}$$

According to (4) and (9), the detailed expression of (11) can be derived out, expressed as

$$\dot{V}_1 = z_1 \left(\dot{x}_1^* - \dot{x}_1\right) = z_1 \left(\dot{x}_1^* - \frac{x_2 - i_{od} + \omega C x_3}{C}\right) \tag{12}$$

The pseudo-current-control-loop reference ${x_2}^*$ is selected to assure $\dot{V}_1 \leq 0$, given by

$$x_2^* = i_{od} - \omega C x_3 + k_1 C z_1 + C\dot{x}_1^* \tag{13}$$

where k_1 is an imported positive constant, serving as the first controller parameter ($k_1 > 0$).

If x_2 is regulated to follow x_2^*, (12) will be transformed to

$$\dot{V}_1 = -k_1 z_1^2 \leq 0 \tag{14}$$

which is always negative definite.

2) STEP TWO: DERIVATION OF THE D-FRAME SWITCHING FUNCTION μ_d

The pseudo inductor current tracking error is defined as

$$z_2 = x_2^* - x_2 \tag{15}$$

The second Lyapunov function is defined as the summation of V_1 and linear-quadratic pseudo-current-loop tracking error z_2, expressed as

$$V_2 = \frac{1}{2}z_1^2 + \frac{1}{2}z_2^2 \tag{16}$$

The time derivative of V_2 is given by

$$\dot{V}_2 = z_1 \dot{z}_1 + z_2 \dot{z}_2 \tag{17}$$

According to (12), (15), detailed expression of (17) can be found, given by

$$\dot{V}_2 = z_1 \left[\dot{x}_1^* - \frac{\left(x_2^* - z_2\right) - i_{od} + \omega C x_3}{C}\right] + z_2 \left(\dot{x}_2^* - \dot{x}_2\right) \tag{18}$$

Substituting (13) and (5) to (18), it gives

$$\dot{V}_2 = -k_1 {z_1}^2 + \frac{z_1 z_2}{C} + z_2 \left(\dot{x}_2^* - \frac{0.5\mu_d E - x_1 + \omega L x_4}{L}\right) \tag{19}$$

The d-frame switching function μ_d is selected to guarantee $\dot{V}_2 \leq 0$, expressed as

$$\mu_d = \frac{2}{E}\left(x_1 - \omega L x_4 + L\dot{x}_2^* + \frac{L}{C}z_1 + k_2 z_2\right) \tag{20}$$

where k_2 is another imported positive constant, serving as the second controller parameter ($k_2 > 0$). (20) transforms (19) into the negative definite format, given by

$$\dot{V}_2 = -k_1 {z_1}^2 - k_2 \frac{z_2^2}{L} \leq 0 \tag{21}$$

B. TWO-STEP BACKSTEPPING DERIVATION IN q FRAME

1) STEP ONE: DERIVATION OF INDUCTOR CURRENT REFERENCE x_4^*

Similarly, load voltage tracking error in q frame is defined as

$$z_3 = x_3^* - x_3 \tag{22}$$

Then, the third Lyapunov function associated with the load voltage tracking error in q frame is defined as

$$V_3 = \frac{1}{2}{z_3}^2 \tag{23}$$

Differentiating (23), it yields out that

$$\dot{V}_3 = z_3 \dot{z}_3 \tag{24}$$

According to (6) and (22), the detailed expression of (24)can be found, expressed as

$$\dot{V}_3 = z_3 \left(\dot{x}_3^* - \dot{x}_3\right) = z_3 \left(\dot{x}_3^* - \frac{x_4 - i_{oq} - \omega C x_1}{C}\right) \tag{25}$$

Then, the pseudo internal current-loop reference ${x_3}^*$ is designed to ensure $\dot{V}_3 \leq 0$, given by

$$x_4^* = i_{oq} + \omega C x_1 + C\dot{x}_3^* + k_3 C z_3 \tag{26}$$

where k_3 is an imported positive constant, serving as the third controller parameter ($k_3 > 0$).

If x_4 is regulated to follow x_4^*, (25) will be transformed to

$$\dot{V}_3 = -k_3 z_3^2 \leq 0 \tag{27}$$

2) STEP TWO: DERIVATION OF THE q-FRAME SWITCHING FUNCTION μ_q

Internal inductor-current-loop tracking error is defined as

$$z_4 = x_4^* - x_4 \tag{28}$$

The fourth Lyapunov function is defined as the summation of V_3, and linear-quadratic current-control-loop tracking error,

$$V_4 = \frac{1}{2}z_3^2 + \frac{1}{2}z_4^2 \tag{29}$$

The first-order time derivative of (29) turns out to be

$$\dot{V}_4 = z_3 \dot{z}_3 + z_4 \dot{z}_4 \tag{30}$$

According to (25), (28), $\dot{V}_4$ can be rewritten as

$$\dot{V}_4 = z_3 \left[\dot{x}_3^* - \frac{\left(x_4^* - z_4\right) - i_{oq} - \omega C x_1}{C}\right] + z_4 \left(\dot{x}_4^* - \dot{x}_4\right) \tag{31}$$

Substituting (26) and (7) to (31), it gives

$$\dot{V}_4 = -k_3 {z_3}^2 + \frac{z_3 z_4}{C} + z_4 \left(\dot{x}_4^* - \frac{0.5\mu_q E - x_3 - \omega L x_2}{L}\right) \tag{32}$$

There exists such a q-frame switching function (μ_q) that could unconditionally guarantee $\dot{V}_4 \leq 0$, given by

$$\mu_q = \frac{2}{E}\left(x_3 + \omega L x_2 + L\dot{x}_4^* + \frac{L}{C}z_3 + k_4 z_4\right) \tag{33}$$

where k_4 is another imported positive constant, serving as the fourth controller parameter ($k_4 > 0$).

(33) transforms (32) into the negative definite format, expressed as

$$\dot{V}_4 = -k_3 {z_3}^2 - \frac{k_4}{L}z_4^2 \leq 0 \tag{34}$$

C. DESIGN OF THE KALMAN FILTER TO ESTIMATE AND FEEDFORWARD THE LOAD CURRENTS FOR LOAD DISTURBANCE REJECTION

(13) and (26) demonstrate that i_{od}, i_{oq} are indispensable to generate the pseudo references x_1^*, x_3^* on the objective of load disturbance suppression. To this end, three load-current sensors and additional *abc-dq* coordinate transformation can be added to generate i_{od}, i_{oq}. However, it increases the implementation cost and sacrifices the system reliability as well. As a better alternative, a Kalman filter can be designed to estimate i_{od}, i_{oq} online [23]. Together with the backstepping control law, it constitutes the composite nonlinear controller.

It is known that the variation of load current can be neglected within one sampling interval [24], expressed as

$$\mathrm{d}i_{od}/\mathrm{d}t = \mathrm{d}i_{oq}/\mathrm{d}t = 0 \tag{35}$$

Combining (35) with (4) and (6), the augmented state-space model of the system can be formulated as

$$\begin{cases} \dot{x} = Ax + B\gamma \\ y = C_n x \end{cases} \tag{36}$$

where

$$A = \begin{pmatrix} 0 & \omega & -\frac{1}{C} & 0 \\ -\omega & 0 & 0 & -\frac{1}{C} \\ 0 & 0 & 0 & 0 \\ 0 & 0 & 0 & 0 \end{pmatrix}, B = \begin{pmatrix} \frac{1}{C} & 0 \\ 0 & \frac{1}{C} \\ 0 & 0 \\ 0 & 0 \end{pmatrix}, x = \begin{pmatrix} v_{od} \\ v_{oq} \\ i_{od} \\ i_{oq} \end{pmatrix}$$

$$C_n = \begin{pmatrix} 1 & 0 & 0 & 0 \\ 0 & 1 & 0 & 0 \end{pmatrix}, \quad \gamma = \begin{pmatrix} i_{Ld} \\ i_{Lq} \end{pmatrix}, \quad y = \begin{pmatrix} v_{od} \\ v_{oq} \end{pmatrix}$$

The investigated system has been proved to be observable since its observability matrix has full rank, given by

$$\mathrm{rank}\,(C_n\ C_nA\ C_nA^2\ C_nA^3)^T = 4 \tag{37}$$

Thus, a Kalman filter can be configured to realize real-time estimation of i_{od}, i_{oq}, as shown in Fig. 3. Its compatible analytic formula is given by

$$\begin{cases} \dot{\hat{x}} = A\hat{x} + B\gamma - G(y - \hat{y}) \\ \hat{y} = C_n\hat{x} \end{cases} \tag{38}$$

where $\hat{x}$ denotes the estimated state variables (x). G is the feedback gain matrix, whose selection is the key for Kalman filter design, which will be illustrated in detail in Section IV.B.

It is worth noting that the use of observers (e.g. Luenberger observers) is typically restricted to the deterministic case. The Kalman filter is preferable for the stochastic case. The investigated POL inverter operates on the SPS that is susceptible to stochastic parametric variation/ measuring errors, making it suitable for the application of the Kalman filter.

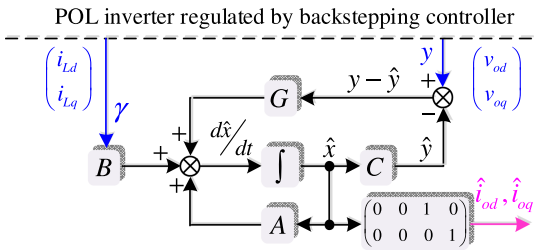

FIGURE 3. Block diagram of the Kalman filter.

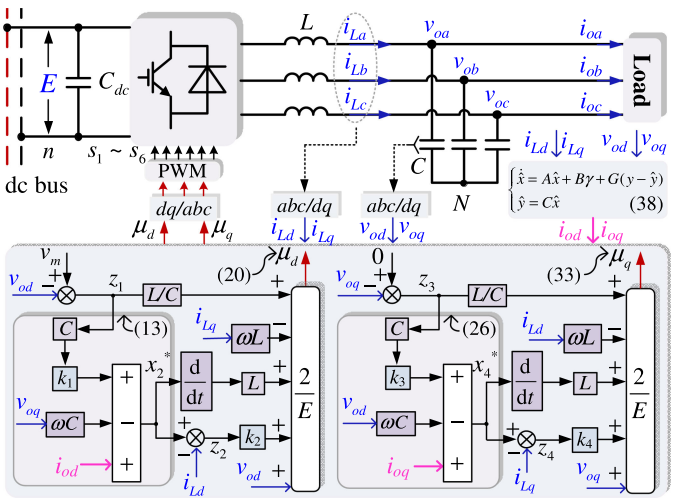

FIGURE 4. Block diagram of the POL inverter in the SPS regulated by the proposed composite backstepping controller.

D. IMPLEMENTATION OF THE PROPOSED COMPOSITE BACKSTEPPING CONTROLLER WITH A KALMAN FILTER

According to (13), (26), (20), (33), a block diagram of the POL inverter in the SPS regulated by the proposed composite backstepping controller is depicted in Fig. 4. Inductor currents are regarded as the pseudo control variables, and x_2^*, x_4^* denote their tracking references. The designed controller has both voltage control-loop errors (z_1, z_3), and pseudo-current-loop errors (z_2, z_4), which means that it inherently has dual control loops. k_1, k_3 are voltage-loop controller gains, and k_2, k_4 are current-loop controller gains. μ_d, μ_q will be compared with the triangular carrier signals in the SPWM modulator, where 'on' and 'off' signals ($s_1 \sim s_6$) are generated for the six switches. The inductor currents (i_{La}, i_{Lb}, i_{Lc}) and load voltages (v_{oa}, v_{ob}, v_{oc}) are measured by sensors. The Kalman filter estimates and feedforward i_{od}, i_{oq} to generate x_2^*, x_4^*, leading to the omission of load-current sensors compared to [17].

IV. ELLIPSE-BASED CONTROLLER GAINS OPTIMIZATION, FEEDBACK GAINS MATRIX SELECTION, AND ROBUSTNESS ANALYSIS

A. PROPOSED INTUITIVE ELLIPSE-BASED STRATEGY TO OPTIMIZE THE CONTROLLER PARAMETERS WITH FULLY CONSIDERATION OF ξ AND ω_n

To tune the controller gains (k_1, k_2, k_3, k_4) quantitatively, dynamics associated with the closed-loop errors (z_1, z_2, z_3, z_4) should be derived out at first. To this end, (15) and (28) are substituted to (4) and (6) respectively, which gives

$$\begin{cases} C\dot{x}_1 = x_2^* - z_2 - i_{od} + \omega C x_3 \\ C\dot{x}_3 = x_4^* - z_4 - i_{oq} - \omega C x_1 \end{cases} \tag{39}$$

The internal current-loop reference (13), (26) are substituted into (39), which yields out that

$$\begin{cases} \dot{z}_1 = -k_1 z_1 + z_2/C \\ \dot{z}_3 = -k_3 z_3 + z_4/C \end{cases} \tag{40}$$

Similarly, substituting the switching functions (20), (33) to (5), (7) respectively, it produces that

$$\begin{cases} \dot{z}_2 = -z_1/C - k_2 z_2/L \\ \dot{z}_4 = -z_3/C - k_4 z_4/L \end{cases} \tag{41}$$

(40), (41) demonstrate the error dynamics in d frame (z_1, z_2) and q frame (z_3, z_4) are inherently decoupled using the proposed approach. d-frame error dynamics will have the symmetric dynamic property to the q-frame counterparts provided that $k_1 = k_3 > 0$ and $k_2 = k_4 > 0$. Under this premise, only k_1 and k_2 are required to be tuned, and (40), (41) can be rewritten as

$$\dot{z}_d = T z_d, \dot{z}_q = T z_q \tag{42}$$

where $z_d = (z_1, z_2)^{\mathrm{T}}$, $z_q = (z_3, z_4)^{\mathrm{T}}$, and

$$T = \begin{pmatrix} -k_1 & 1/C \\ -1/C & -k_2/L \end{pmatrix} k_1 > 0, k_2 > 0 \tag{43}$$

The characteristic polynomial of matrix T is given by

$$\det(\lambda I - T) = \lambda^2 + \left(k_1 + \frac{k_2}{L}\right)\lambda + \frac{k_1 k_2}{L} + \frac{1}{C^2} \tag{44}$$

Since the closed-loop error dynamics have been reduced to a typical second-order system, its compatible damping ratio (ξ) and natural resonant frequency (ω_n) could serve as the physical indicators to do the controller gains' optimization.

It is known that ξ, ω_n directly manifests the steady-state and dynamic characteristics of the closed-loop system. Larger ω_n means the faster dynamic response of the system, while larger ξ implies more damping can be provided for the system. To be more specific, larger ω_n signifies that the state variables will be regulated to track their references with less convergence time. Larger ξ leads to less total harmonic distortion in steady-state and less overshoot during transients.

Initially, (44) is written as the characteristic-polynomial format of a typical second-order system, given by

$$\det(\lambda I - T) = \lambda^2 + 2\xi\omega_n\lambda + {\omega_n}^2 \tag{45}$$

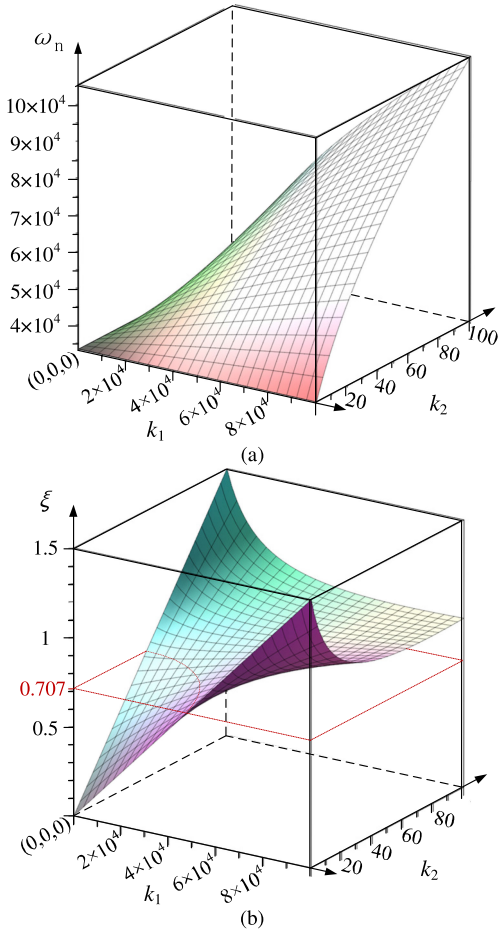

FIGURE 5. Variation of the physical indicators as controller parameters increase ($k_1 > 0$, $k_2 > 0$). (a) ω_n as k_1 and k_2 increase; (b) ξ as k_1 and k_2 increase.

$\det(\lambda I - T) = 0$ has two solutions, denoted as $\lambda_{1,2}$:

$$\lambda_{1,2} = -\xi\omega_n \pm \omega_n\sqrt{\xi^2 - 1} \tag{46}$$

where ξ, ω_n are derived out to be

$$\xi = \frac{CLk_1 + Ck_2}{2\sqrt{k_1 k_2 LC^2 + L^2}}, \omega_n = \sqrt{\frac{k_1 k_2}{L} + \frac{1}{C^2}} \tag{47}$$

Fig. 5 (a), (b) depict the scenario where ξ, ω_n vary as the increase of k_1, k_2 based on (47). It shows that ω_n monotonically increases as k_1 or k_2 increases. However, ξ has a comparatively non-monotonic relationship to k_1 or k_2. Although k_1, k_2 can be roughly selected using Fig. 5, it is hard to take ξ, ω_n into account simultaneously, no less to say the parameter optimization.

As a better alternative, this paper proposes an intuitive ellipse-based optimization strategy for k_1 and k_2 from a geometrical point of view, which could ensure optimal system damping and maximized dynamic response. To strike a trade-off between better dynamic response and overshoot during

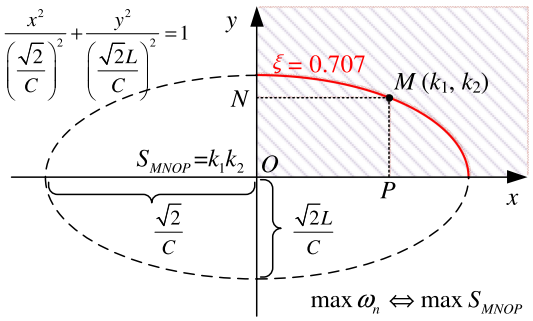

FIGURE 6. An intuitive interpretation of the controller gains' optimization process from a geometric point of view.

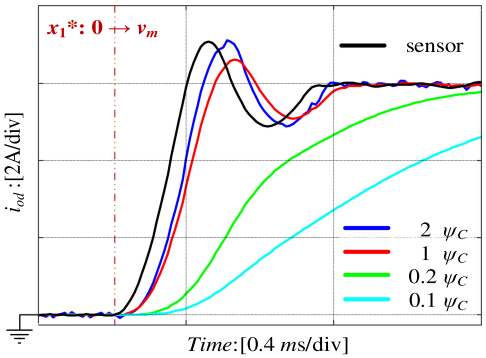

FIGURE 7. The tracking performance of the Kalman filter as ψ_O varies.

transients, ξ is fixed to be the optimal damping ratio [14], [25]:

$$\xi = \frac{CLk_1 + Ck_2}{2\sqrt{k_1k_2LC^2 + L^2}} = \frac{\sqrt{2}}{2} \approx 0.707 \tag{48}$$

After mathematical transformation (48) can be rewritten as

$$\frac{{k_1}^2}{\left(\sqrt{2}/C\right)^2} + \frac{{k_2}^2}{\left(\sqrt{2}L/C\right)^2} = 1\,(k_1 > 0, k_2 > 0) \tag{49}$$

Note that L is no less than 1 H (1000 mH) in a real-world physical system. Therefore, (50) always holds, and (49) turns out to be a standard equation of an ellipse in the x-y Cartesian coordinate system where the two focuses of the ellipse are located on the x-axis, depicted as Fig. 6.

$$\sqrt{2}/C > \sqrt{2}L/C > 0 \tag{50}$$

As seen in Fig. 6, the controller parameters' combination $M(k_1, k_2)$ that guarantees the optimal damping ratio $\xi = 0.707$ are located at the first quadrant part of the ellipse (marked in red) since $k_1 > 0$ and $k_2 > 0$.

Without loss of generality, mathematically equivalent parametric equation of (49) can be expressed as

$$k_1 = \frac{\sqrt{2}}{C}\cos\theta, k_2 = \frac{\sqrt{2}L}{C}\sin\theta, \text{where } \theta \in \left[0, \frac{\pi}{2}\right] \tag{51}$$

According to (47), ω_n has a proportional relationship to the area of the rectangle, denoted as $S_{MNOP} = k_1k_2$. Using (51), S_{MNOP} can be rewritten as

$$S_{MNOP} = k_1k_2 = \frac{\sqrt{2}}{C}\cos\theta \cdot \frac{\sqrt{2}L}{C}\sin\theta = \frac{L}{C^2}\sin 2\theta \tag{52}$$

$$\omega_n = \sqrt{\frac{S_{MNOP}}{L} + \frac{1}{C^2}} = \frac{1}{C}\sqrt{\sin 2\theta + 1} \tag{53}$$

(53) shows that the maximum of S_{MNOP} and ω_n can be achieved if and only if $\theta = \pi/4$, which gives

$$\max S_{MNOP} = \frac{L}{C^2}\sin 2\theta\Big|_{\theta=\frac{\pi}{4}} = \frac{L}{C^2} \Rightarrow \max \omega_n = \frac{\sqrt{2}}{C} \tag{54}$$

Under this premise, the optimal controller parameters (k_1^*, k_2^*) can be determined accordingly, given by

$$\begin{cases} k_1^* = \sqrt{2}\cos\theta/C\big|_{\theta=\frac{\pi}{4}} = 1/C \\ k_2^* = \sqrt{2}L\sin\theta/C\big|_{\theta=\frac{\pi}{4}} = L/C \end{cases} \tag{55}$$

B. QUANTITATIVE SELECTION OF THE FEEDBACK GAIN MATRIX G OF THE KALMAN FILTER AIDED BY ELLIPSE-OPTIMIZED STRATEGY

A well-acknowledged classical approach selects the observer feedback gain matrix G via following formula,

$$G = -PC_n{}^{-1}R^{-1} \tag{56}$$

where matrix P can be obtained by solving the Riccati equation, given by

$$PA^T + AP - PC^TR^{-1}CP + Q = 0 \tag{57}$$

Here, Q and R are two design matrixes. Q is positive definite and R is semi-positive definite, whose selection depends on trial and errors [24].

As seen in (46) $\xi\omega_n$ measures the distance between $\lambda_{1,2}$ and the imaginary axis. Using the proposed ellipse-optimized strategy, $\xi\omega_n$ has been maximized to (Ψ_C), given by

$$\psi_C = 0.707 \times \max \omega_n = 0.707\sqrt{2}/C \tag{58}$$

Closed-loop Poles of the Kalman filter can be calculated out by solving det(sI-A-GC_n) = 0. The dominant poles of Kalman filter should have such real parts (Ψ_O) that are (1∼2) times of Ψ_C, which provides a quantitative guideline for Q, R selection.

In Fig. 7, the tracking performance of the Kalman filter is considered under x_1* step when supplying a linear resistive load. It demonstrates that the selection of Ψ_O is a trade-off between convergence speed and disturbance susceptibility. When $\Psi_O = 0.1\Psi_C$ or $0.2\Psi_C$, it takes a long time to converge. If $\Psi_O = 2\Psi_C$, the estimated i_{od} tracks the i_{od} measured by current sensors instantly, while it is undesirably disturbed by circuit noise.

C. ROBUSTNESS ANALYSIS OF THE PROPOSED CONTROL SCHEME UNDER PARAMETRIC VARIATIONS AND MEASUREMENT ERRORS

Matrix A, B in (38) are dependent on the system parameters that are susceptible to measurement errors and plant parametric variation for a real-world system. To take account of this effect, (38) is rewritten as

$$\begin{cases} \dot{\hat{x}} = A\hat{x} + B\gamma - G(y - \hat{y}) + \Gamma\hat{x} \\ \hat{y} = C_n\hat{x} \end{cases} \tag{59}$$

where Γ is an unknown 4-by-4 matrix, modeling the lumped uncertainty due to parametric variation and measurement errors.

According to (36) and (59), the error dynamics of the Kalman filter considering external disturbance is given by

$$\dot{z} = (A + \Gamma + GC_n)\, z \tag{60}$$

where z denotes the state estimation error: $z = \hat{x}$ - x. Inspired by [24], a Lyapunov function V_o is formulated to investigate the stability of the Kalman filter, given by

$$V_o = z^T P^{-1} z \tag{61}$$

whose first-order time derivative is derived as

$$\dot{V}_o = 2z^T P^{-1} \dot{z} \tag{62}$$

Substituting (60) and (56) to (62), it gives

$$\begin{aligned} \dot{V}_o(z) &= 2z^T P^{-1} \left(A + \Gamma - PC_n{}^{-1}R^{-1}C_n\right) z \\ &= 2z^T P^{-1} \left(AP + \Gamma P - PC_n{}^{-1}R^{-1}C_nP\right) P^{-1} z \\ &= z^T P^{-1}(AP + PA^T + \Gamma P + P\Gamma^T - 2PC_n{}^{-1}R^{-1}C_nP)P^{-1}z \end{aligned} \tag{63}$$

According to (57), (63) can be rewritten as

$$\dot{V}_o = z^T P^{-1} \left(-Q + \Gamma P + P\Gamma^T - PC_n{}^{-1}R^{-1}C_nP\right) P^{-1} z \tag{64}$$

Negative definiteness of (64) can be rigorously guaranteed one the premise that:

$$\Gamma P + P\Gamma^T < Q + PC_n{}^{-1}R^{-1}C_nP \tag{65}$$

Therefore, for any scale of parametric mismatch and measurement errors satisfying (65), $\dot{V}_o < 0$ can be still ensured, and z will exponentially convergence to zero.

Another Lyapunov function V_c is formulated to prove the stability of the closed-loop system (42), given by

$$V_c = z_d{}^H z_d + z_q{}^H z_q \tag{66}$$

where $(\bullet)^H$ denotes the conjugate transpose matrix of $(\bullet)$. The time derivative of (66) is given by

$$\dot{V}_c = \dot{z}_d^H z_d + z_d{}^H \dot{z}_d + \dot{z}_q^H z_q + z_q{}^H \dot{z}_q \tag{67}$$

Substituting (42) to (67), it gives

$$\begin{aligned} \dot{V}_c &= (Tz_d)^H z_d + z_d{}^H T z_d + \left(Tz_q\right)^H z_q + z_q{}^H T z_q \\ &= z_d{}^H \left(T^H + T\right) z_d + z_q{}^H \left(T^H + T\right) z_q \end{aligned} \tag{68}$$

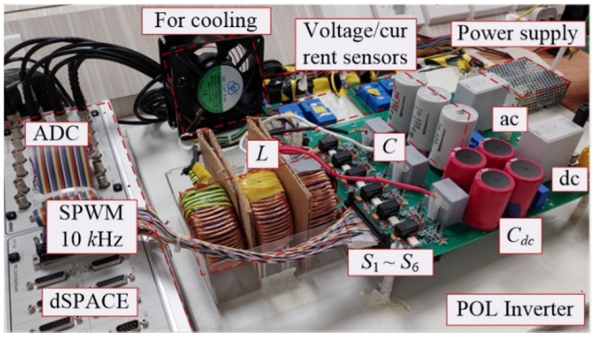

FIGURE 8. Experimental setup.

TABLE 1. Nominal System Parameters

E	ω	f_s	L	C	v_m	C_{dc}	Z
350 V	100π	10 kHz	1 mH	30 μF	115 V	470 μF	19.25 Ω

where $T^H + T$ cancels out all their off-diagonal entries.

According to (43), (68) can be rewritten as

$$\dot{V}_c = z_d{}^H \begin{pmatrix} -2k_1 & 0 \\ 0 & -2k_2/L \end{pmatrix} z_d + z_q{}^H \begin{pmatrix} -2k_1 & 0 \\ 0 & -2k_2/L \end{pmatrix} z_q < 0 \tag{69}$$

which demonstrates that L, C does not affect the system stability if $k_1, k_2 > 0$. Meanwhile, L, C, k_1, k_2 can vary at a large range without deteriorating the stability of the closed-loop system.

V. EXPERIMENTAL RESULTS

A 1 kW-rated POL inverter prototype is fabricated for experimental verification, as seen in Fig. 8. The dSPACE functions as the controller. System parameters are listed in Table 1. According to (55), the optimal controller gains are calculated out to be: $k_1^* = k_3^* = 3.33 \times 10^4$, $k_2^* = k_4^* = 33.33$. Ψ_O is selected as around $1\Psi_C$, where G is selected as $G = 10^4 \times (6.664, -0.0314, -3.333, 0; 0.0314, 6.666, 0, -3.3326)^T$.

A. EFFECTIVENESS OF THE PROPOSED ELLIPSE-OPTIMIZED CONTROLLER GAINS SELECTION STRATEGY

In Fig. 9(a), k_1 and k_2 are both selected smaller than the optimal controller gains. According to Fig. 5(b), inadequate controller gains will lead to poor system damping, complying well with the experimental results shown in Fig. 9(a). In Fig. 9(b), k_1 increase to $10k_1{}^*$, and k_2 remain unchanged compared to the counterparts in Fig. 9(a). Fig. 5(b) predicts that an increase of k_1 would lead to an increase of damping ratio, which also fulfills the experimental result shown in Fig. 9(b).

The designed optimal controller gains can theoretically fix the damping ratio to 0.707. Under this premise, the natural frequency has been maximized to achieve the best dynamic performance. Fig. 9(c) presents the experimental results with the optimal controller gains. Compared with Fig. 9(a), Fig. 9(c)

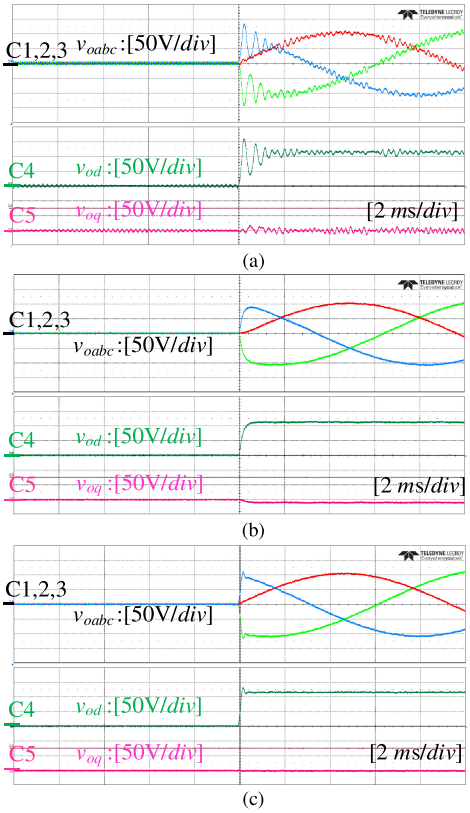

FIGURE 9. Control performance of the proposed approach under reference step (x_1*: 0 → v_m) with different set of controller gains. (a) $k_1 = 0.1k_1^*$, $k_2 = 0.1k_2^*$; (b) $k_1 = 0.1k_1^*$, $k_2 = 10k_2^*$; (c) $k_1 = k_1^*$, $k_2 = k_2^*$.

has effectively suppressed the oscillation and overshoot during transients. In comparison with Fig. 9(b), Fig. 9(c) takes less transient time to track the reference step (x_1*: 0 → v_m).

B. ROBUSTNESS TESTS UNDER PLANT PARAMETRIC VARIATIONS

To test the robustness of the proposed control scheme against parametric variations and reference step, ±50% L and ±50% C scale of filter parametric variation have been considered, where x_1^* steps from 0 to v_m and $x_3^*$is fixed to 0. As seen in Fig. 10, the variation of LC parameters mainly affects the THD of the load voltage, while the stability of the closed-loop system does not get deteriorated. Larger L or C contributes to suppressing the THD of the load voltage. Every time x_1^* steps from 0 to v_m, the load voltage (x_1) soon tracks x_1^* with negligible rise time and overshoot. To summarize, Fig. 10 demonstrates that the proposed control scheme can at least withstand ±50% L, C scale of plant parametric variation.

C. PERFORMANCE EVALUATION UNDER LINEAR/NONLINEAR LOAD STEP, REFERENCE STEP, OVERLOAD AND RECOVERY

Four case studies have been conducted to evaluate the performance of the proposed control scheme. As seen in Fig. 11

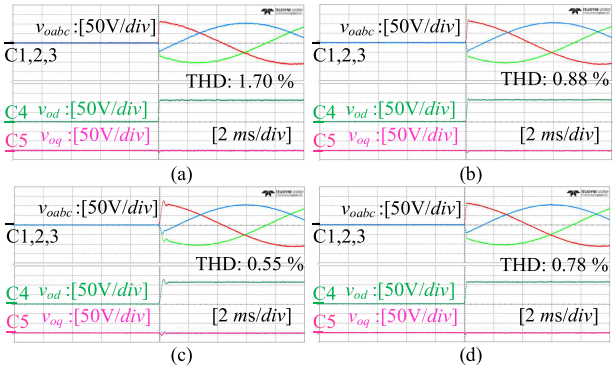

FIGURE 10. Experimental results of the robustness tests. (a) −50%L, −50%C; (b) +50%L, −50%C; (c) +50%L, +50%C; (d) −50%L, +50%C.

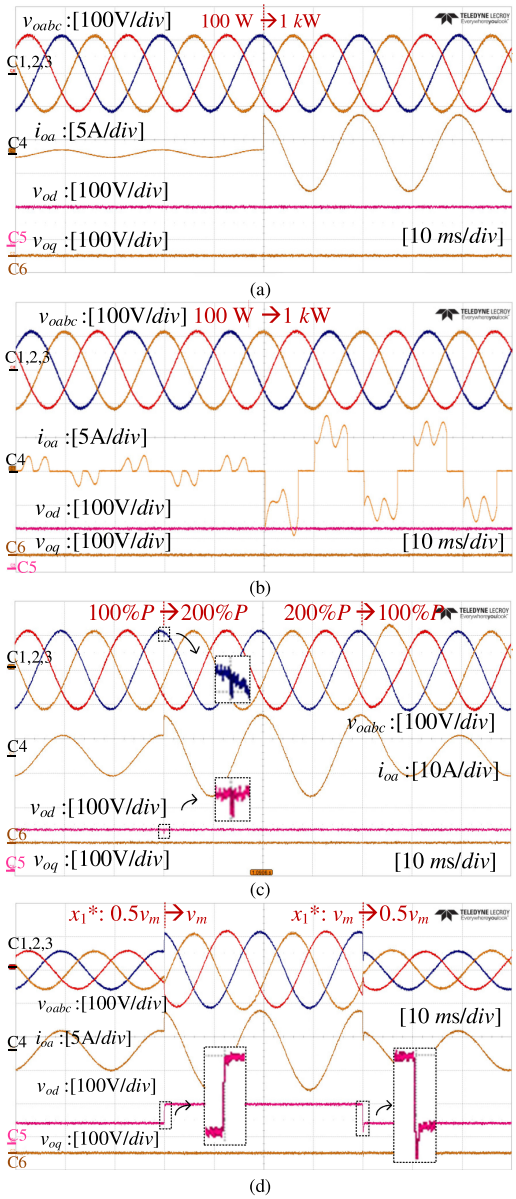

FIGURE 11. Performance evaluation of the proposed control scheme. (a) linear load step; (b) nonlinear load step; (c) overload & recovery; (d) reference step.

TABLE 2. Comparisons Between Existed Lyapunov-Based Control Schemes and the Proposed Approach

References	[17]	[18]	This paper
States' feedbacks	Extended dual loops	Inherent dual loops	Inherent dual loops
Lyapunov function (V)	Conventional	Adaptive weighted	Recursive
Large-signal stability	Ensured (conditional)	Ensured	Ensured
Load-current sensors	Required	0	0
Controller tuning	Root locus	Jacobian matrix $A(t)$	Explicit formulas
Controller gains	$K_i = 2\times10^3$ $K_v = 4.9\times10^3$	$\sigma = 100$ $\gamma = 0.1$	$k_1^* = 3.33\times10^4$, $k_2^* = 33.33$
THD %	1.16	0.97	0.79
3rd harmonic %	0.07	0.10	0.03
5th harmonic %	0.07	0.09	0.11
7th harmonic %	0.05	0.14	0.03
Robustness against LC mismatch	Not reported	At least ±50 %	At least ±50 %

(a), (b), (c), the POL inverter is under linear load step, nonlinear load step from 100 W to 1 *k*W, and overload condition respectively, while the three-phase load voltage always remains pure sinusoidal. It shows that the proposed controller is capable to suppress such a scale of load disturbance due to load uncertainty and nonlinearity. Fig. 11 (d) demonstrates the great tracking performance of the controller under x_1^* steps up/down. It always shows that *d*-*q* decoupled control has been realized.

D. COMPARISONS BETWEEN EXISTED LYAPUNOV-BASED APPROACHES AND THE PROPOSED CONTROL SCHEME

Existed Lyapunov-based approaches and the proposed control scheme are compared in Table 2 and Fig. 12. [17] is devised based on the conventional Lyapunov function (V), where V is formulated as the linear quadratic tracking errors associated with the inductor current and capacitor voltage. [17] is an extended dual-loop control scheme where the capacitor voltage feedback is artificially imported. Global large-signal stability of the system can be ensured on the premise that the imported voltage feedback gain is larger than a specific lower bound. The load-current sensor is indispensable in [17].

Both [18] and the proposed approach are inherently dual-loop control schemes, that can rigorously guarantee the global large-signal stability of the system. The key for [18] design is based on an adaptive weighted Lyapunov function, whose design requires genuine expertise. In comparison, the proposed approach selects the Lyapunov function step by step in a recursive manner using the backstepping approach, which is systematic. With an adaptive law, [18] has saved load-current sensors. However, as seen in Fig. 12, the load voltage undergoes a certain amount of voltage sag during the load step. The proposed approach obviates the load-current sensor with the help of the Kalman filter.

One common obstacle of [17] and [18] is that the controller gains selection is indeed a trial-and-error process. Although

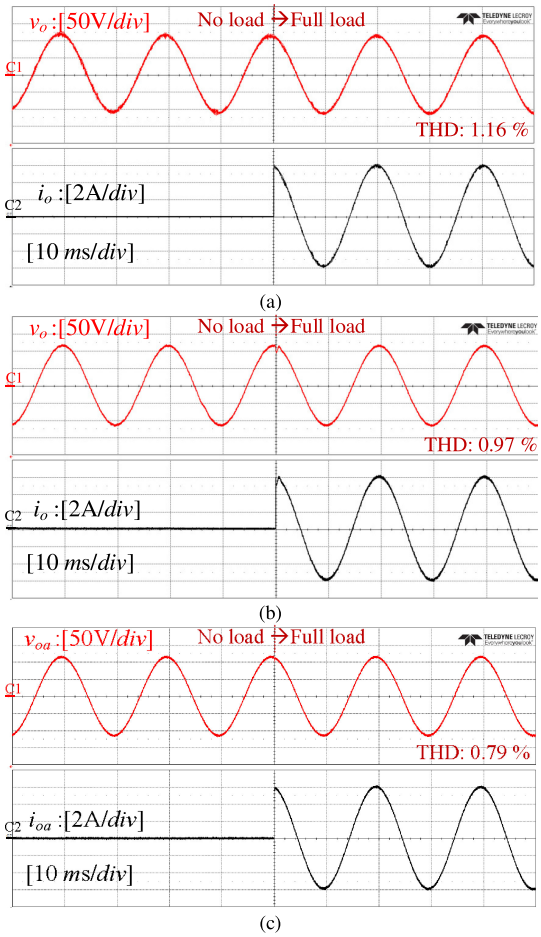

FIGURE 12. Performance evaluation under linear load step. (a) [17]; (b) [18]; (c) the proposed approach.

the root-locus technique in [17], the eigenvalues of the Jacobian matrix in [18] may provide certain help for controller gains selection, it lacks explicit formulas to tune the controller gains. In comparison, the optimal controller gains in this paper are quantitatively calculated out, which is straightforward and time saving for practical implementation. THD of the load voltage using the proposed approach is around 0.79%, which is lower than 1.16% using [17] and 0.97% using [18].

VI. CONCLUSION

The proposed composite backstepping controller inherently has dual control loops to achieve both great steady-state and dynamic performance. Meanwhile, it can rigorously guarantee the large-signal stability of the POL inverter with great robustness against at least a ±50% scale of plant parametric variations. A Kalman filter is further designed to estimate the load currents and feedforward them to the backstepping controller, leading to the omission of load-current sensors compared to [17]. The proposed strategy realizes *d*-*q* decoupled control, resulting in a dimension-reduced second-order system. [17] and [18] do not present any explicit formulas for controller gains selection, where trial-and-error methods are inevitable.

In this paper, the optimal controller gains are quantitatively calculated out via explicit formulas to achieve the optimal system damping and maximized dynamic response, which can be intuitively interpreted via an ellipse-based strategy from a geometrical point of view. Rigorous stability proof and robustness analysis of the system is also provided. THD % of the load voltage using the proposed control scheme is around 0.79%, which is lower than that using [17] and [18].

REFERENCES

[1] A. Vicenzutti, D. Bosich, G. Giadrossi, and G. Sulligoi, "The role of voltage controls in modern all-electric ships: Toward the all-electric ship," *IEEE Electrif. Mag.*, vol. 3, no. 2, pp. 49–65, Jun 2015.

[2] R. Heydari, M. Gheisarnejad, M. H. Khooban, T. Dragicevic, and F. Blaabjerg, "Robust and fast voltage-source-converter (VSC) control for naval shipboard microgrids," *IEEE Trans. Power Electron.*, vol. 34, no. 9, pp. 8299–8303, Sep. 2019.

[3] Z. Ma, X. Zhang, J. Huang, and B. Zhao, "Stability-constraining-dichotomy-solution-based model predictive control to improve the stability of the power conversion system in the MEA," *IEEE Trans. Ind. Electron.*, vol. 66, no. 7, pp. 5696–5706, Jul. 2019.

[4] T. Dragičević, "Dynamic stabilization of DC microgrids with predictive control of point-of-load converters," *IEEE Trans. Power Electron.*, vol. 33, no. 12, pp. 10872–10884, Dec. 2018.

[5] M. Mellincovsky, V. Yuhimenko, M. M. Peretz, and A. Kuperman, "Low-frequency DC-link ripple elimination in power converters with reduced capacitance by multiresonant direct voltage regulation," *IEEE Trans. Ind. Electron.*, vol. 64, no. 3, pp. 2015–2023, Mar. 2017.

[6] C. S. Ting, Y. N. Chang, and Y. Y. Chen, "Backstepping direct thrust force control for sensorless pmlsm drive," *IET Electr. Power Appl.*, vol. 13, no. 3, pp. 322–331, Mar. 2019.

[7] X. Zhang, Q. C. Zhong, V. Kadirkamanathan, J. He, and J. Huang, "Source-side series-virtual-impedance control to improve the cascaded system stability and the dynamic performance of its source converter," *IEEE Trans. Power Electron.*, vol. 34, no. 6, pp. 5854–5866, Jun. 2019.

[8] M. Kabalan, P. Singh, and D. Niebur, "Large signal Lyapunov-based stability studies in microgrids: A review," *IEEE Trans. Smart Grid*, vol. 8, no. 5, pp. 2287–2295, Sep. 2017.

[9] H. P. Ren, J. T. Fan, and O. Kaynak, "Optimal design of a fractional-order proportional-integer-differential controller for a pneumatic position servo system," *IEEE Trans. Ind. Electron.*, vol. 66, no. 8, pp. 6220–6229, Aug. 2019.

[10] H. T. Nguyen, E. K. Kim, I. P. Kim, H. H. Choi, and J. W. Jung, "Model predictive control with modulated optimal vector for a three-phase inverter with an LC filter," *IEEE Trans. Power Electron.*, vol. 33, no. 3, pp. 2690–2703, Mar. 2018.

[11] M. Pichan, H. Rastegar, and M. Monfared, "Deadbeat control of the stand-alone four-leg inverter considering the effect of the neutral line inductor," *IEEE Trans. Ind. Electron.*, vol. 64, no. 4, pp. 2592–2601, Apr. 2017.

[12] N. Altin, S. Ozdemir, H. Komurcugil, and I. Sefa, "Sliding-mode control in natural frame with reduced number of sensors for three-phase grid-tied LCL-interfaced inverters," *IEEE Trans. Ind. Electron.*, vol. 0046, no. c, pp. 2903–2913, Apr. 2018.

[13] S. Jiang, D. Cao, Y. Li, J. Liu, and F. Z. Peng, "Low-THD, fast-transient, and cost-effective synchronous-frame repetitive controller for three-phase UPS inverters," *IEEE Trans. Power Electron.*, vol. 27, no. 6, pp. 2994–3005, Jun. 2012.

[14] I. Sefa, S. Ozdemir, H. Komurcugil, and N. Altin, "Comparative study on Lyapunov-function-based control schemes for single-phase grid-connected voltage-source inverter with LCL filter," *IET Renew. Power Gener.*, vol. 11, no. 11, pp. 1473–1482, Sep. 13, 2017.

[15] H. Komurcugil, S. Member, N. Altin, and S. Ozdemir, "Lyapunov-function and proportional-resonant-based control strategy for single-phase grid-connected vsi with LCL filter," *IEEE Trans. Ind. Electron.*, vol. 63, no. 5, pp. 2838–2849, May 2016.

[16] I. Sefa, S. Ozdemir, H. Komurcugil, and N. Altin, "An enhanced Lyapunov-function based control scheme for three-phase grid-tied VSI with LCL filter," *IEEE Trans. Sustain. Energy*, vol. 3029, no. 2, pp. 504–513, Apr. 2019.

[17] H. Komurcugil, N. Altin, S. Ozdemir, and I. Sefa, "An extended Lyapunov-function-based control strategy for single-phase UPS inverters," *IEEE Trans. Power Electron.*, vol. 30, no. 7, pp. 3976–3983, Jul. 2015.

[18] J. He, C. C. Y. John, X. Zhang, Z. Li, and Z. Liu, "An adaptive dual-loop Lyapunov-based control scheme for a single-phase UPS inverter," *IEEE Trans. Power Electron.*, vol. 8993, no. c, pp. 1–1, Sep. 2020.

[19] S. Yousefizadeh, J. D. Bendtsen, N. Vafamand, M. H. Khooban, F. Blaabjerg, and T. Dragicevic, "Tracking control for a dc microgrid feeding uncertain loads in more electric aircraft: Adaptive backstepping approach," *IEEE Trans. Ind. Electron.*, vol. 66, no. 7, pp. 5644–5652, Jul. 2019.

[20] Q. Xu, C. Zhang, C. Wen, and P. Wang, "A novel composite nonlinear controller for stabilization of constant power load in DC microgrid," *IEEE Trans. Smart Grid*, vol. 10, no. 1, pp. 752–761, Jan. 2019.

[21] D. Karimipour and F. R. Salmasi, "Stability analysis of AC microgrids with constant power loads based on Popov's absolute stability criterion," *IEEE Trans. Circuits Syst. II Express Briefs*, vol. 62, no. 7, pp. 696–700, Jul. 2015.

[22] T. Dragičević and M. Novak, "Weighting Factor design in model predictive control of power electronic converters: An artificial neural network approach," *IEEE Trans. Ind. Electron.*, vol. 66, no. 11, pp. 8870–8880, Nov. 2019.

[23] D. Simon, *Optimal State Estimation-Kalman, H-infinity, and Nonlinear Approaches*. Cleveland, OH, USA: Cleveland State Univ., 2006.

[24] E. Kim, F. Mwasilu, H. H. Choi, and J. Jung, "An observer-based optimal voltage control scheme for three-phase UPS systems," *IEEE Trans. Ind. Electron.*, vol. 62, no. 4, pp. 2073–2081, Apr. 2015.

[25] W. S. Levine, *The Control Handbook (Three Volume Set)*. Cleveland, OH, USA: CRC Press, 2018.

JINSONG HE (Student Member, IEEE) was born in Hubei Province, China, in 1997. He received the B.S. degree in electrical engineering and its automation from Wuhan University, Wuhan, China, in 2018. From January 2018 to June 2018, he accomplished his final year project in Clean Energy Research, Nanyang Technological University (NTU), Singapore. He is currently working toward the Ph.D. degree with the School of Electrical and Electronic Engineering, NTU. His research interests include power electronics stability and control.

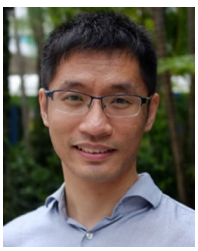

XIN ZHANG (Senior Member, IEEE) received the Ph.D. degree in automatic control and systems engineering from the University of Sheffield, U.K., in 2016 and the Ph.D. degree in electronic and electrical engineering from the Nanjing University of aeronautics & astronautics, China, in 2014. Currently, he is an Assistant Professor of power engineering with the School of Electrical and Electronic Engineering of Nanyang Technological University. He was the Postdoctoral Research Fellow from January to September 2017 at the City University of Hong Kong and the Research Associate from February 2014 to December 2016 at the University of Sheffield. Dr Xin Zhang has received the highly-prestigious Chinese National Award for Outstanding Students Abroad in 2016. His research interests include in power electronics, power system, and advanced control theory, together with their applications in various sectors.